

**Military Technical College
Kobry El-Kobbah,
Cairo, Egypt.**



**17th International Conference
on Applied Mechanics and
Mechanical Engineering.**

WINGLET CANT AND SWEEP ANGLES EFFECT ON AIRCRAFT WING PERFORMANCE

E. S. Abdelghany ^{*}, E. E. Khalil ^{**}, O. E. Abdellatif ^{***} and G. ElHariri ^{****}

ABSTRACT

A winglet is a device used to improve the efficiency of aircraft by lowering the lift induced drag caused by wingtip vortices. It is a vertical or angled extension at the tips of each wing. Winglets improve efficiency by diffusing the shed wingtip vortex, which in turn reduces the drag due to lift and improves the wing's lift over drag ratio, Winglets increase the effective aspect ratio of a wing without adding greatly to the structural stress and hence necessary weight of its structure. In this research, a numerical validation procedure (by FLUENT ®, computational fluid dynamics software with The Spalart-Allmaras turbulence model) is described for determination and estimation aerodynamic characteristics of three dimension subsonic rectangular wing (with NACA653218 airfoil cross section). It was observed that at the present work a good agreement between the numerical study and the experimental work. This paper describes a CFD 3-dimensional winglets analysis that was performed on a Cessna wing of NACA2412 cross sectional airfoil. The wing has span 13.16 m, root chord 1.857 m, tip chord 0.928 m, sweep angle 11 degree and taper ratio 0.5. The present study shows wing without winglet and wing with winglet at cant angle 0, 30 and 45 degree and sweep angle 0, 20 and 40 degree. A CFD simulation performs by to compare of aerodynamics characteristics of lift coefficient C_L , drag coefficient C_D and lift to drag ratio, L/D lift, pathlines and pressure contours. The models run at a Mach number of 0.2 at sea level. The pressure and temperature of air at this height are 101.325 kpa and 288.2 K respectively. The results show the wing with winglet can be increase lift by ratio approximately 12%. The wing with winglet can decrease drag by ratio approximately 23%. The wing with winglet can increase lift to drag, L/D by about 13% along different phases of flight.

KEY WORDS

Winglet, computational fluid dynamics, Cant and Sweep Angles, Aerodynamics characteristics

^{*} PHD student, Institute of Aviation Engineering, Cairo , Egypt.
^{**} Professor of Mechanical Engineering, Cairo University, Egypt.
^{***} Professor of Mechanical Engineering. Benha University, Egypt.
^{****} Assistant Professor of Mechanical Engineering. Cairo University, Egypt.

NOMENCLATURE

List of symbols

b	= Span length of wing (m)
C	= Chord length (m)
C_L	= Lift coefficient
C_D	= Drag coefficient
C_M	= Moment coefficient
E	= Total energy of a fluid
	= particle constant
h	= Enthalpy (J/kg)
L	= Length (m)
	= Lift force (N)
M	= Mach number
	= Pitching moment (N.m)
S	= Reference area
P	= Pressure value
R	= Radius (m)
Re	= Reynolds number, $Re = \rho U C / \mu$
t	= Time (sec)

v	= Instantaneous y direction velocity (m/sec)
T	= Temperature (K)
x, y, z	= Cartesian coordinate components

Greek Letters

α	= Angle of attack (deg.)
γ	= Sweep angle of winglet (deg.)
ϵ	= Turbulence dissipation rate
μ	= Dynamic viscosity (kg/m.sec)
ρ	= Density (kg/m ³)

List of Abbreviations

AOA	= Angle of attack (deg.)
AR	= Aspect ratio of wing
CFD	= Computational Fluid Dynamics

INTRODUCTION

The winglet, which is airfoil operating just like a sailboat tacking upwind. The winglet Produce a forward thrust inside the circulation field of the vortices and reduce their strength. Weaker vortices mean less drag at the wingtips and lift is restored. Improved wing efficiency translates to more payloads, reduced fuel consumption, and a longer cruising range that can allow an air carrier to expand routes and destinations. Winglets application is one of the most noticeable fuel economic technologies on aircraft [1], [2] and [3]. Most of the commercial long range aircraft has installed winglet to decrease the induce drag to save more fuel [4], [5], [6] and [7], this feature can be also found on the bird. Bird use its feather at wingtip as "multiple winglet" [8] and [9], which can be seen Figure 1. Each feather has different angle respect to the wing, and they are passively adapted to the different flight conditions, which is different from the fixed angle winglet in the conventional aircraft.

From [10], parabolic shaped configuration winglets at cant angles 45 and 55 degrees are analyzed on rectangular NACA 2412 airfoil sections using CFD analysis at Reynolds number 200000 and 400000 to compare aerodynamic characteristics. It is found that the L/D ratio increases by 13.447 and the coefficient of lift (CL) increases by 1.958%. A maximum reduction in coefficient of drag (CD) is by 10.125% and thereby reducing fuel consumption of the aircraft. CFD 3-dimensional winglets analysis was described on a rectangular wing of NACA653218 airfoil section, [11]. The wing dimensions are a span of 660 mm (b) and a chord of 121 mm (c) and is analyzed for two shape configurations, semicircle and elliptical. This paper presented elliptical winglet with cant angle of 45 degree that has the highest lift-to-drag ratio by about 17.62% from wing without winglet. The aerodynamic characteristic are

described in the aircraft wing model with and without bird feather like winglet, [8]. The experimental result shows 25-30 % reductions in drag coefficient and 10-20 % increase in lift coefficient by using bird feather like winglet for angle of attack of 8 degree. Numerical investigation of five configurations of winglets is described and preliminary indications of their aerodynamic performance are provided, [12]. Moreover, using advanced multi-objective design optimization software an optimal one-parameter winglet configuration was determined that simultaneously minimizes drag, maximizes lift, improved lift-to-drag ratio (the maximum value increased by up to a 15%), significantly increased range, improved take-off and landing performance, reduced engine emissions, shortened climbing time, reduced turbulence behind the aircraft and reduced the time gap between the landings.

GOVERNING EQUATIONS

The air flow is modelled as 3-D compressible viscous flow. Thus the governing equations are the continuity equation together with x- y and z- Navier-Stokes equations for a compressible flow. Turbulence is modelled by the Spalart-Allmaras model. The complete system of equations is presented here in differential form, (FLUENT® documentation [13] and [14]). The governing equations in this model are:

A. Continuity equation in vector form:

$$\frac{\partial \rho}{\partial t} + \nabla \cdot (\rho \vec{V}) = 0$$

B. Momentum equation in vector form:

$$\nabla \cdot (\rho \vec{v} \vec{v}) = -\nabla p + \nabla \cdot (\vec{\tau}) + \vec{F}$$

C. Energy Conservation Equation:

$$\frac{\partial (\rho E)}{\partial t} + \nabla \cdot (\vec{v} (\rho E + p)) = \nabla \cdot \left[k_{eff} \nabla T - \sum_j h_j \vec{J}_j + (\vec{\tau}_{eff} \cdot \vec{v}) \right] + S_h$$

VALIDATION CODE PROCEDURES

The computational steps in this project consist of three stages. The project began from pre-processing stage of geometry setup and grid generation. The geometry of the model and the grid was generated by GAMBIT. The second stage was computational simulation by FLUENT solver using Finite Volume Approach. Finally is the post-processing stage where the aerodynamics characteristics of rectangular wing with NACA65s218airfoil are computed. From CFD model we determine lift, drag, pitching moment coefficient, pressure contours, velocity contours and pathlines around wing at all AOA.

Geometry and Grids

First draw rectangular wing with NACA 653218 airfoil by using Gambit. The wing has a chord length of 121 mm and a semi-span of 330 mm. In order to obtain accurate lift, drag, and pitching moment on wing, grids near the wing volume must be dense enough and computed fields must be large enough to satisfy far field boundary conditions. 3D Unstructured tetrahedral mesh is used for complex shape of winglet. In present work multi-block unstructured grid is used to increase grids near wing volume by creating blocks 1, 2, 3, 4, 5 and 6, as shown in Figure 2.

The numerical model of a rectangular wing with NACA65₃218 airfoil section with boundary condition is illustrated in Figure 3.

The mesh is generated using GAMBIT® 2.3.16 as a pre-processor and mesh generator. It is very crucial that the grid size be as small as possible at boundaries (at the wing walls [block 1]). However, it is also important that the grid volumes be as large as possible to reduce the solution time and allocated memory [blocks 2, 3, 4, 5, 6], as shown in Figure 4.

Grid dependency check

The first step in performing a CFD simulation should be to investigate the effect of the mesh size on the solution results. Generally, a numerical solution becomes more accurate as more cells are used, but using additional cells also increases the required computer memory and computational time. To examine the independency of the results to cell number, seven kinds of mesh are generated. The results of these seven meshes are shown in Fig. 5, Lift coefficient with number of grid cell at angle of attack (12°).

In order to save time when running the computations, the grid with the smallest number of cells displaying an independent solution would be used for the calculations. This is seen to be the case for a grid with around 1500000 cells. The Rectangular wing with NACA65₃218airfoil section model was used to verify the work done by [15], [8] and [11]. Compare the results of the numerical model by Spalart-Allmaras model to those of the experimental and numerical models. Figure 6 shows the lift coefficient (C_L) with angle of attack from 0 degree to angle of attack 12 degree of numerical and experimental studies, plotted on the same axes and scale for comparison. For comparison, it is found maximum error by Spalart-Allmaras model is about 20%. The results show good agreement of lift, as shown in Fig.6, and drag coefficient with the corresponding values in the experimental and numerical models.

It is selected Cessna Citation Mustang aircraft. The Cessna Citation Mustang is a low-wing aircraft with retractable tricycle landing gear and a T-tail. Two Pratt & Whitney Canada (P&WC) PW615F turbofan engines are pylon-mounted on the rear fuselage.

Effect of winglet with cant and sweep angles

The Cessna citation mustang wing has a span of 13.16 m, a root chord of 1.857 m, a tip chord of 0.928 m, a sweep angle of 11 degree and a taper ratio of 0.5, as shown in Fig.7.

The setup for analysis consists of three cases: a simple Cessna swept back wing, no winglets, the same wing with winglet at Cant angle (θ) and Sweep angle (γ). The selected geometry of the winglet is taken as the generalized a Cant-and a Sweep-angle (WCSA) (also called wing with winglet Cant-sweep angle) type. From Table 1 and Fig.8, the Cant angle (θ) is varied of 0° , 30° and 45° and the sweep angle (γ) is varied of 0° , 20° and 40° . The wing has a chord length of 1.857 m with NACA2412airfoil is extruding by 5.7 m. The wing taper ratio is 0.5 and leading edge sweep back angle 11 degree to create wing volume. The winglets have the same aerofoil of wing and length 20% of semi span with sharp edge connection with wingtip, see in Fig. 8. These nine cases all have the same initial conditions. Since wingtip vortices are more prevalent at take-off conditions for low speed and high lift conditions, the wings will be run at a Mach number of 0.2 at sea level. The pressure and temperature of air at this height are 101.325 kpa and 288.2 K respectively.

Table 1: Studied types of shaped of winglet.

		Cant angle (θ)		
		0°	30°	45°
Sweep angle of winglet(γ)	0°	Winglet with cant 0° and sweep 0° (WCSA-00-00)	Winglet with cant 30° and sweep 0° (WCSA-30-00)	Winglet with cant 45° and sweep 0° (WCSA-45-20)
	20°	Winglet with cant 0° and sweep 20° (WCSA-00-20)	Winglet with cant 30° and sweep 20° (WCSA-30-00)	Winglet with cant 45° and sweep 20° (WCSA-45-20)
	40°	Winglet with cant 0° and sweep 40° (WCSA-00-40)	Winglet with cant 30° and sweep 40° (WCSA-30-40)	Winglet with cant 45° and sweep 40° (WCSA-45-40)

RESULTS AND DISCUSSION

It is studied the wing without and with winglet. Parametric study is performed on winglet by changing the Cant angle (θ) and the Sweep angle (γ). From CFD model we determine lift, drag, pressure contours and pathlines around wing at all AOA.

Lift Coefficient, C_L Analysis

At the end of the analysis of many cases for different winglet angles, it can conclude that the case of the highest lift coefficient is WCSA-00-00. The coefficient of lift versus angle of attack for Wing with winglet at cant angle 0, 30, 45 degrees and sweep angle 0 degrees, studied in the present investigation are shown in Fig. 9 at a Mach number of 0.2. In Table 2 and Figure 9 are observed lift increases with increases in angle of attack. Wings with winglets have higher lift coefficient, C_L than wing without winglet about 5% to 12% with angle of attack. The WCSA-00-00 has highest lift coefficient Improvements at AOA 0 and 4 degree. WCSA-30-00 and WCSA-45-00 Lift coefficient at AOA 8 and 12 degree are higher than other wings.

Table 2: Lift Coefficient, C_L Wing with winglet at cant angle 0, 30, 45 degree and sweep angle 0 degree.

Winglet configuration	$\alpha=0^\circ$	$\alpha=4^\circ$	$\alpha=8^\circ$	$\alpha=12^\circ$
WCSA-00-00	0.15004	0.41157	0.64555	0.81786
WCSA-30-00	0.146983	0.410894	0.647421	0.819315
WCSA-45-00	0.145856	0.410166	0.646656	0.822806

Drag Coefficient, C_D Analysis

At the end of the analysis of many cases for different winglet angles, it can conclude that the case of the lowest lift coefficient is WCSA-45-40. The coefficient of Drag versus angle of attack of the wing with winglet at a sweep 0, 20 and 40 degree of constant cant angle 45 degree, studied in the present investigation are shown in Fig. 10 at a Mach number of 0.2. From the figure, it is observed that the drag increases with increase in angle of attack. From Table 3 shows by increasing sweep angle, drag coefficient, C_D is decreasing. The WCSA-45-40 has lower drag coefficient, C_D than wing without winglet by about 21% to 23% with angle of attack. The WCSA-45-20 has the second lower drag coefficient, C_D than wing without winglet by about 11% to 14% with angle of attack. The WCSA-45-00 gives the third lowest drag coefficient, C_D than wing without winglet by about 1.5% to 3.5% with angle of attack.

Table 3: Drag Coefficient, C_D for wing with winglet at sweep 0, 20 and 40 degree at constant cant angle 45 degree.

Winglet configuration	$\alpha=0^\circ$	$\alpha=4^\circ$	$\alpha=8^\circ$	$\alpha=12^\circ$
WCSA-45-00	0.01611	0.02501	0.04839	0.0836
WCSA-45-20	0.01378	0.02144	0.04178	0.07263
WCSA-45-40	0.01233	0.01925	0.03743	0.06499

Lift-To-Drag Ratio, C_L/C_D Analysis

At the end of the analysis of many cases for different winglet angles, we can conclude that the case of the highest lift coefficient is WCSA-45-40. The lift-to-drag ratio, C_L/C_D for wing with winglet at sweep 0, 20 and 40 degrees at constant cant angle 45 degree, studied in the present investigation are shown in Fig. 11 at a Mach number of 0.2. The optimal AOA is 4 degree and the maximum C_L/C_D is WCSA-45-40 at the optimal angle of attack. Table 4 shows that the wings with winglets have higher lift-to-drag ratio than wing without winglet. The WCSA-45-40 has the highest lift-to-drag ratio, C_L/C_D by about 10.5 to 13% along the angle of attack more than wing without winglet. This is followed by WCSA-45-20 which is the second highest lift-to-drag ratio, C_L/C_D by about 8.7 to 11.5 % along angle of attack more than the

wing without winglet. The WCSA-45-00 gives the third lowest lift-to-drag ratio, C_L/C_D about 8.5 to 10 % with angle of attack more than wing without winglet.

Table 4: Lift-To-Drag Ratio, C_L/C_D for wing with winglet at sweep 0, 20 and 40 degree at constant cant angle 45 degree.

Winglet configuration	$\alpha=0^\circ$	$\alpha=4^\circ$	$\alpha=8^\circ$	$\alpha=12^\circ$
WCSA-45-00	9.05404	16.3993	13.3628	9.8418
WCSA-45-20	9.46195	17.1464	13.8164	10.0836
WCSA-45-40	9.47269	17.2401	14.0151	10.2892

Static Pressure Contours

Figure 12 shows upper surface static pressure contours for Wing with winglet at cant angle 0, 30, 45 degree and sweep angle 0 degree. At angle of attack 0 degree, the upper surface will create a lower static pressure. The losses in pressure due to connection between wing and winglet decrease with increase cant angle and the pressure is more uniform, that's decreasing drag. At angle of attack 12 degree, the high intensity blue area located on the upper surface decrease but lift is still capable of generating, but most of the total force is directed backward as drag. For all angle of attack, it shows the low-pressure region on the middle of wing, but at the tip of the wing, the minimum pressure is greater than the minimum pressure at the root. The lower pressure decreases from root to tip of wing then pressure increases along winglet to reach the atmosphere pressure, that's reducing vortices at wing tip.

Figure 13 shows lower surface static pressure contours for Wing with winglet at cant angle 0, 30, 45 degree and sweep angle 0 degree. When the angle of attack increases, the lower surface will create a higher static pressure. The high intensity red area located on the lower surface suggests high lift is generated at high angle of attack, α . For all angle of attack, it shows the high-pressure region is on the middle of wing, at the tip of the wing; the high pressure is lower than the high pressure at the root. The higher pressure decreases from root to tip and along winglet to reach the atmosphere pressure.

Pathlines

The difference pressure between upper and lower surfaces of wing makes the vortex. When angle of attack is increasing, the difference in pressure is increasing then the vortex and the drag of wing is increasing. The wing alone presents only one large vortex at the wingtip as expected. The rotation sense is easily deductible from pathlines. From it, one can realize that effectively fluid has a wide trend to go from lower to upper surface. Figure 14 represents the pathlines view of flow over the studied wing without winglet at Mach number of 0.2 and angle of attack of 12 degree. These pathlines are focused at the wingtip where trailing vortices occurs. The trailing vortices occur greatly at maximum angle of attack when an airplane takes off.

Figure 15 represent the pathlines view of flow over the studied WCSA-45-40 at Mach number of 0.2 and angle of attack of 12 degree. These pathlines are focused at the wingtip where trailing vortices occurs. The small trailing vortices are found in winglet tip and connection. by increasing cant angle the losses due to connection between wing and winglet decrease, that's decreasing trailing vortices and drag. The trailing vortices occur greatly at maximum angle of attack when an airplane takes off. It is found the trailing vortices reducing because, the presence of the winglet, eliminates the downwash. The drag decreases in case of wing with winglet than for wing without winglet.

CONCLUSIONS

By using CFD to predict the performance of the Numerical Model of wing, huge amount of time and money can be saved before testing the wing in the wind tunnel. Calculations show that trends of numerically-simulated curves are in excellent agreement with trends of experimentally-obtained ones.

- From the CFD solution, the pathlines show how wingtip vortices occur and how wing with winglet decrease wingtip vortices at high angle of attack. The cant angle and sweep angle improved drag coefficient by decreasing about 23% and lift to drag ratio by increasing about 13% compared with wing without winglet.
- The lowest drag coefficient; C_D is for case WCSA-45-40 than another winglets.
- The optimal AOA is 4 degree for this type of flow conditions and the maximum lift to drag ratio, C_L/C_D is 17,24 for WCSA-45-40 at an optimal angle of attack.
- Finally it is found that each winglet configuration at a particular AOA had a different lift coefficient, C_L , drag coefficient, C_D and lift to drag ratio, L/D values, indicating that fixed winglets do not provide optimum aircraft performance at different phases of flight.

REFERENCES

- [1] Sankrithi, M. K., Frommer, V. B.J., "Controllable Winglets", United States Patent Document, Patent No. US2008/0308683, 2008.
- [2] Larson, G., "How Things Work: Winglets." Air & Space Smithsonian. Last modified September 2001. <http://www.airspacemag.com/flight-today/wing.html>.
- [3] Brady, C., "Advanced Blended/Advanced Technology Winglets." The Boeing 737 Technical Site", Last modified February 24, 2013.
- [4] Thiede, P., "Aerodynamic Drag Reduction Technologies", Proceedings of the CEAS/DragNet European Drag Reduction Conference, 19-21 June 2000, Potsdam, Germany vol. 76: Springer Verlag, 2001.
- [5] The Aviation Partners Boeing Co. United States Patent. "Blended Winglet", September 1994.
- [6] http://www.boeing.com/commercial/757family/pf/pf_facts.html.
- [7] ICAO, Operational opportunities to minimise fuel use and reduce emissions, proposed ICAO Circular, CAEP/5-IP/4, 2014.

- [8] Hossain, A., Rahman, A., Iqbal, P., Ariffin, M. and Mazian, M. "Drag Analysis of an Aircraft Wing Model with and without Bird Feather like Winglet", International Journal of Aerospace and Mechanical Engineering, pp. 8-13, 2012.
- [9] Smith, M. J., Komerath N., Ames, R., and Wong, O., "Performance Analysis OF A Wing with Multiple Winglets" American Institute of Aeronautics and Astronautics (AIAA-2407), 2001.
- [10] Arvind, P., and Ayush, O., "Application of CFD Simulation in the Design of a Parabolic Winglet on NACA 2412" Proceedings of the World Congress on Engineering, Vol II, London, U.K., 2014.
- [11] Azlin, M. A., Mat Taib, C. F., Kasolang, S. and Muhammad, F. H. "CFD Analysis of Winglets at Low Subsonic Flow", World Congress on Engineering, Vol. 1, 2011, pp. 1-5, 2011.
- [12] Nikola, N.G., Boško, P.R., George, S.D., Vladimir, B.P., "Commercial Aircraft Performance Improvement Using Winglets", Computational Mechanics, 6th European Conference on Computational Fluid Dynamics, Barcelona, Spain, VOL. 43, No 1, 2015.
- [13] Versteeg, H., and Malalasekera, W. "An Introduction to Computational Fluid Dynamics: The Finite Volume Method" Longman, 1995.
- [14] FLUENT Documentation. © Fluent Inc. (2005).
- [15] Beechook, A. and Wang, J., "Aerodynamic Analysis of Variable Cant Angle Winglets for Improved Aircraft Performance", Proceedings of the 19th International Conference on Automation & Computing, Brunel University, London, UK, 13-14 September, 2013.
- [16] Jones, Robert T., "Improving The Efficiency Of Smaller Transport Aircraft", 14th Congress of the International Council of the Aeronautical Sciences, Proceedings, Vol. 1, Toulouse, Fr, 1984

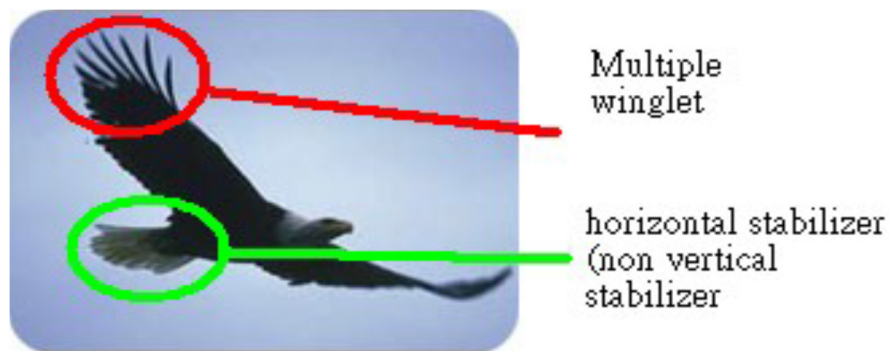


Fig. 1: A bird's wing during flight [2].

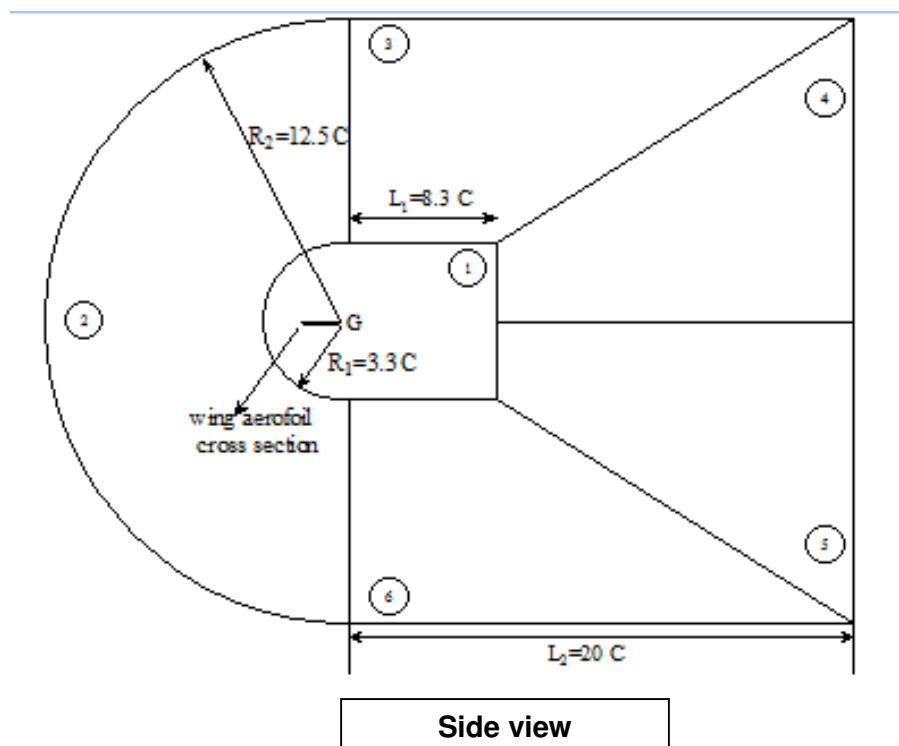


Fig. 2: Side view computed flow field for Rectangular wing with NACA653218 airfoil section.

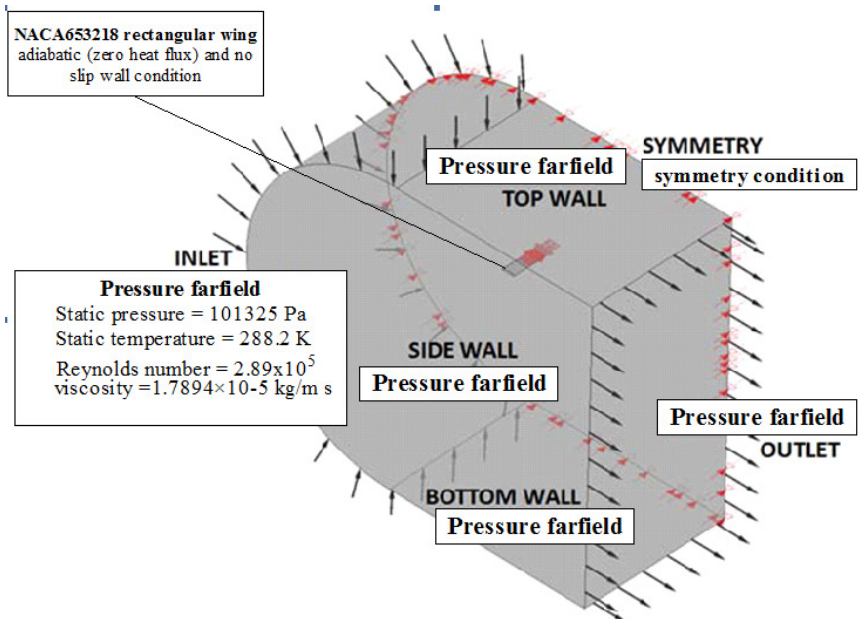


Fig. 3: Numerical model of NACA653218 rectangular wing.

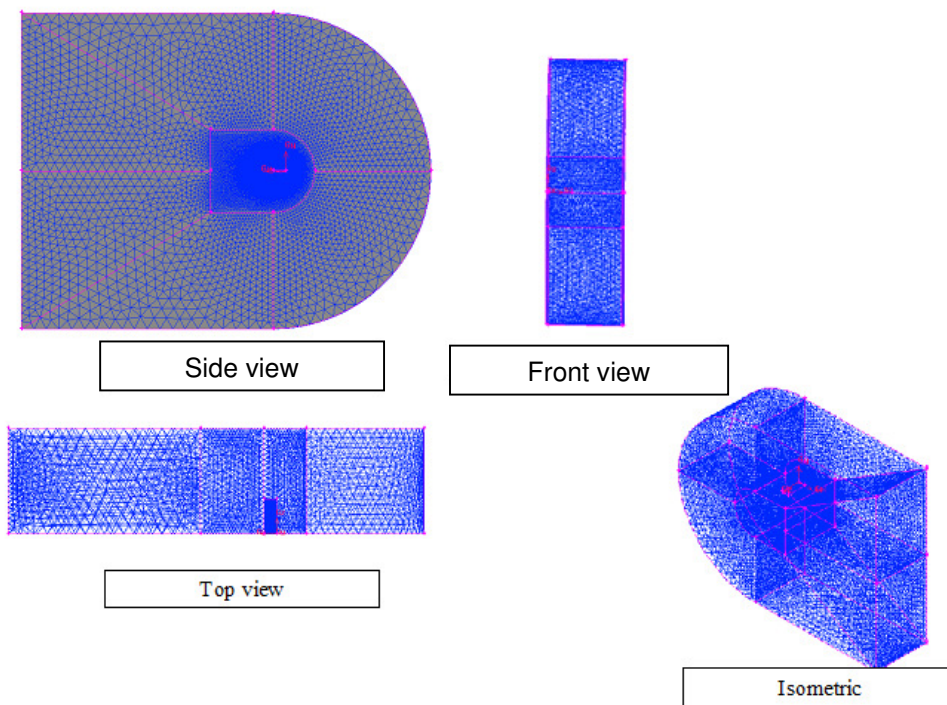


Fig. 4: Views of meshed control volume.

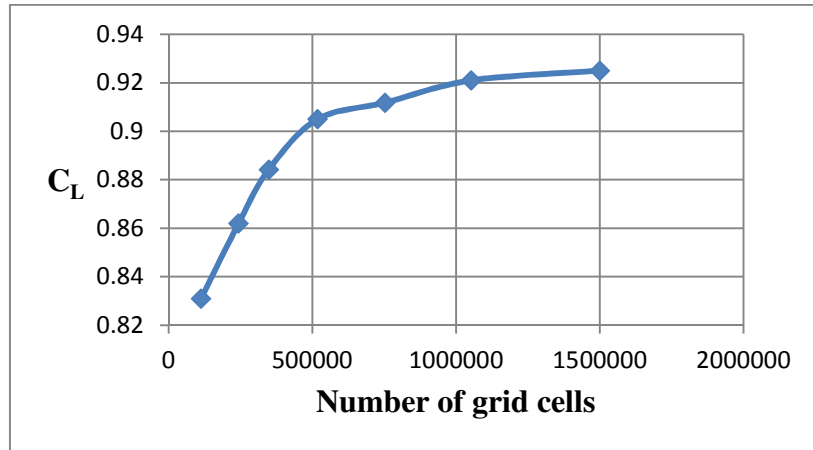


Fig. 5: Curve of lift coefficient at angle of attack 12° against number of grid cells.

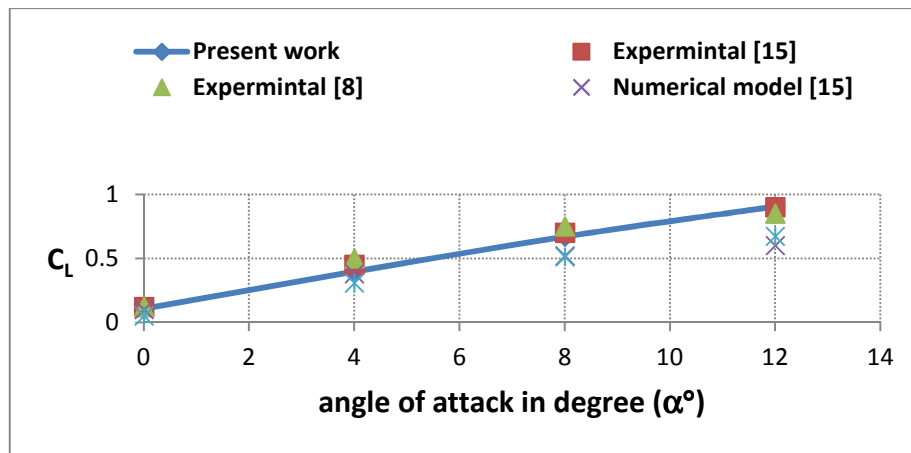


Fig. 6: Numerical results of C_L in comparison to corresponding experimental results.

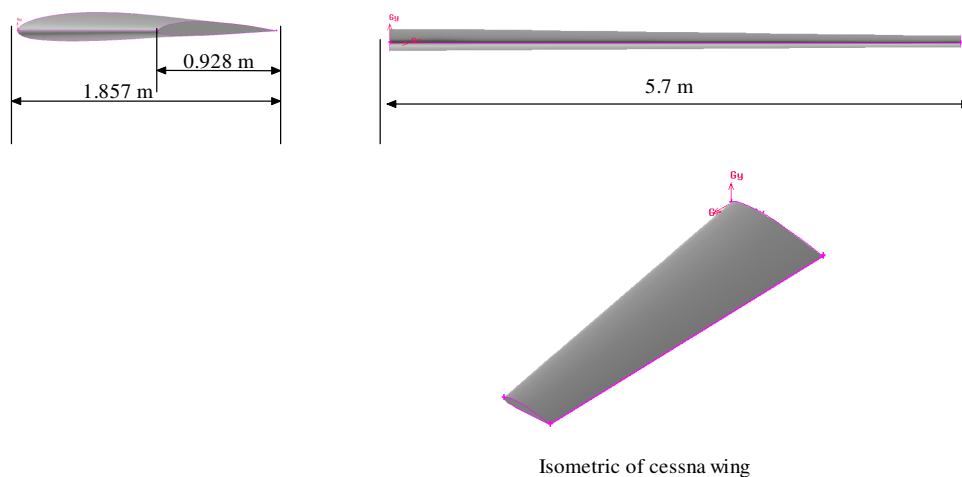


Fig. 7: Cessna wing views and dimensions with NACA2412airfoil section.

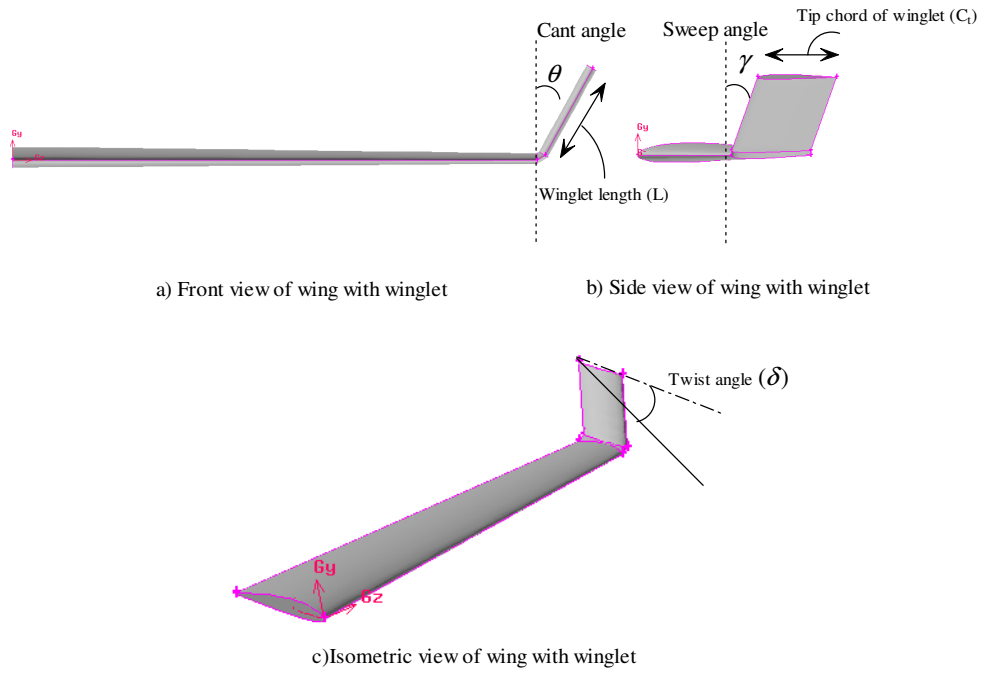


Fig. 8: Winglet shape parameters.

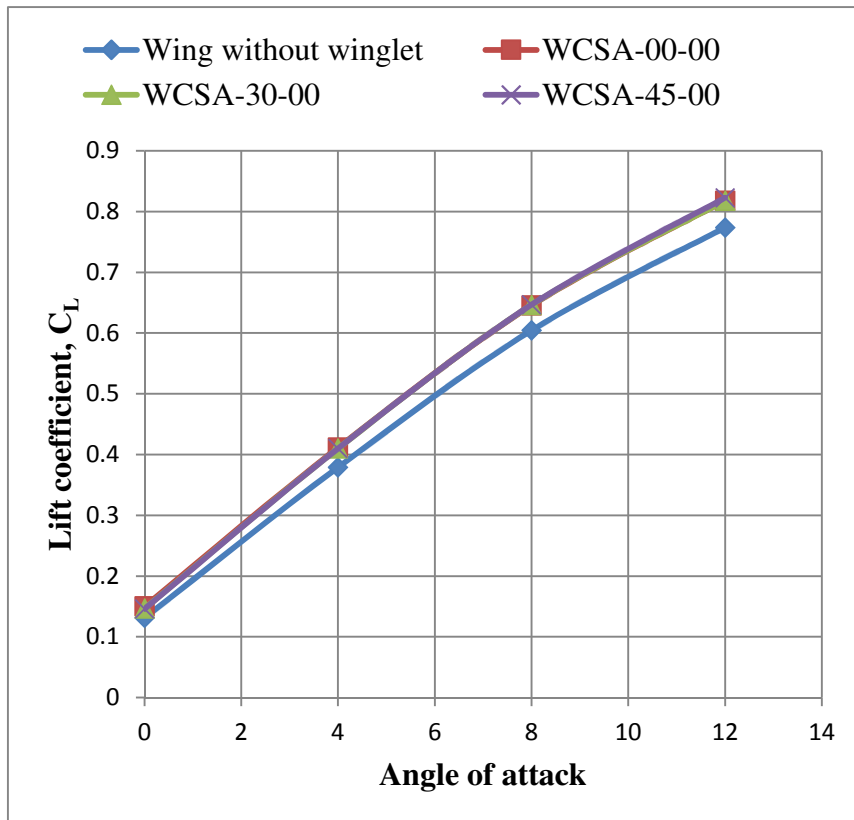


Fig. 9: Lift coefficient, C_L versus angle of attack, α , for Wing with winglet at cant angle 0, 30, 45 degree and sweep angle 0 degree with $M=0.2$ at sea level.

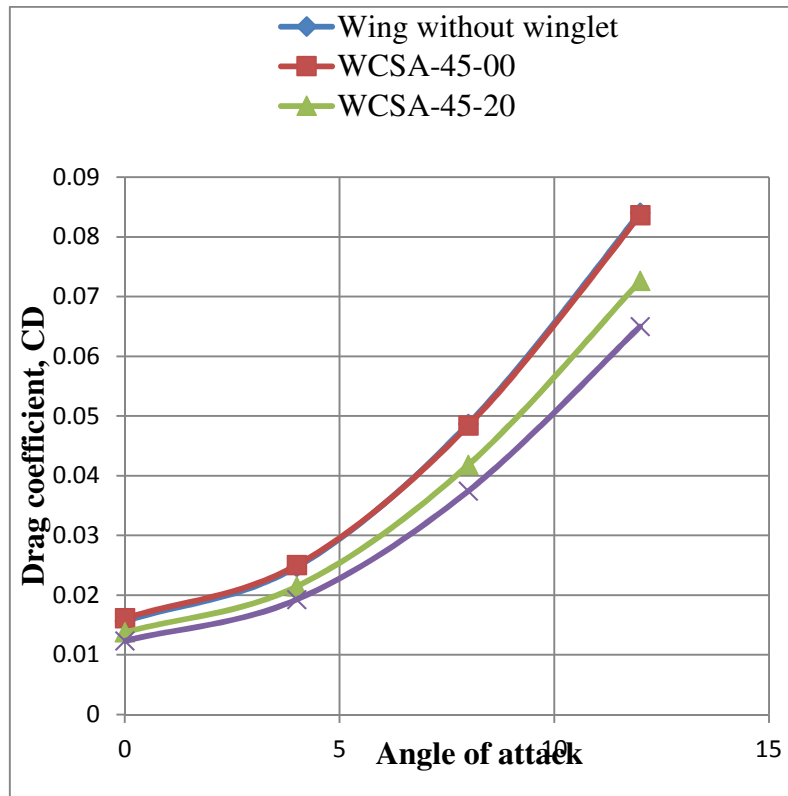


Fig. 10: Drag coefficient, C_D versus angle of attack, α , for wing with winglet at sweep 0, 20 and 40 degree at constant cant angle 45 degree with $M=0.2$ at sea level.

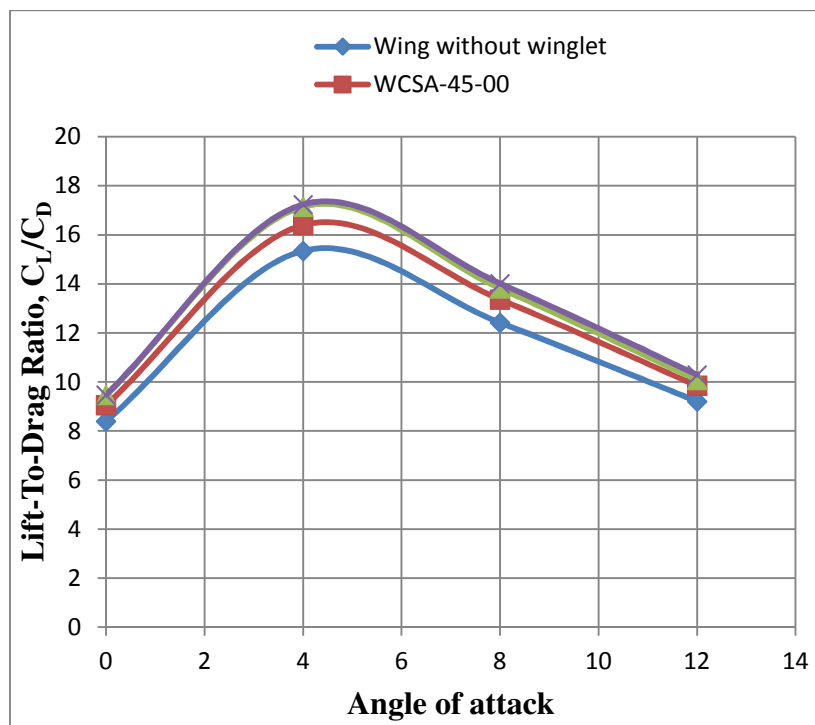


Fig. 11: Lift-to-drag ratio, C_L/C_D at various angle attacks, α , for wing with winglet at sweep 0, 20 and 40 degrees at constant cant angle 45 degree with $M=0.2$ at sea level.

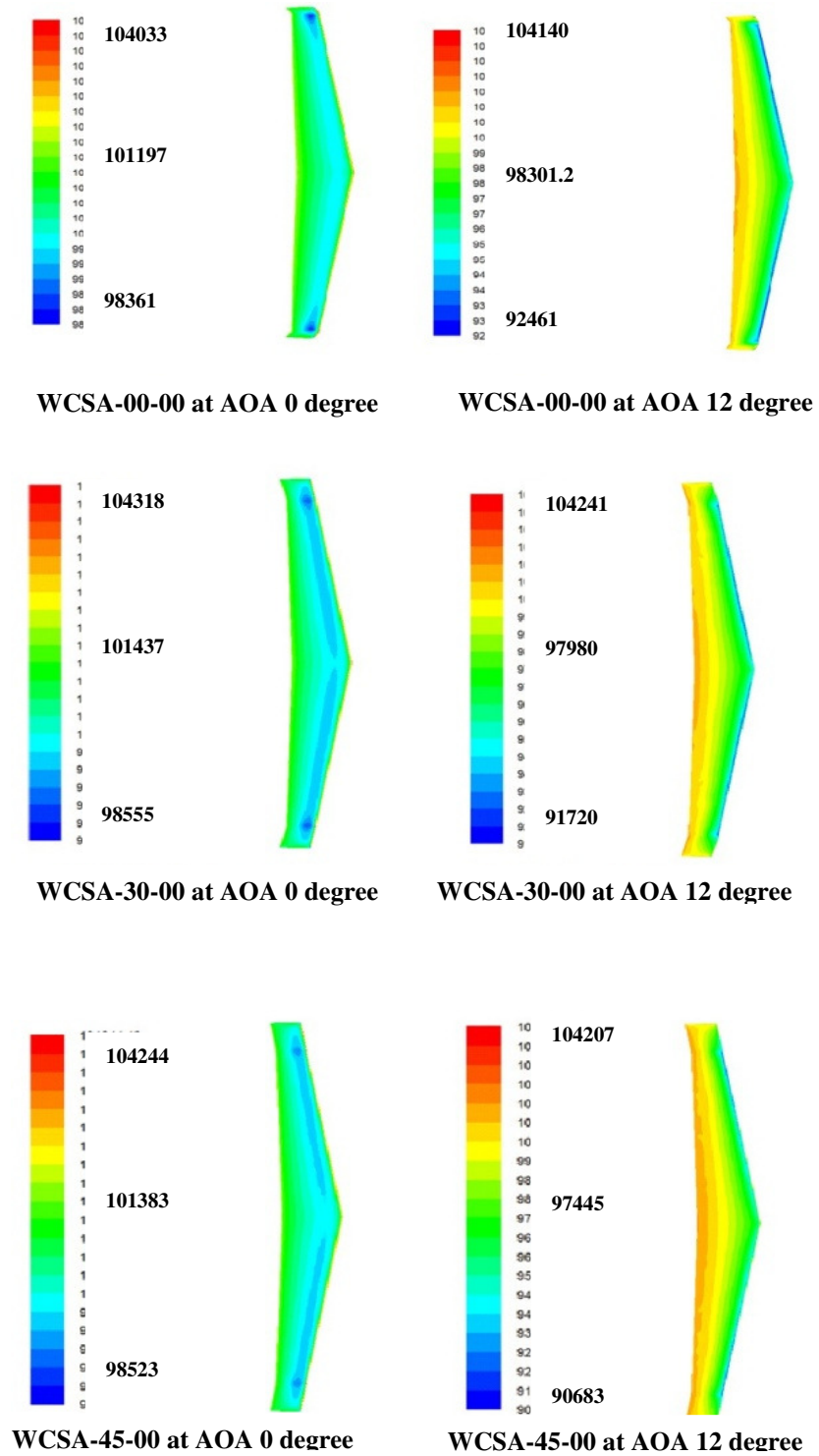


Fig. 12: Upper surface static pressure contours for Wing with winglet at cant angle 0, 30, 45 degree and sweep angle 0 degree with $M=0.2$ at sea level.

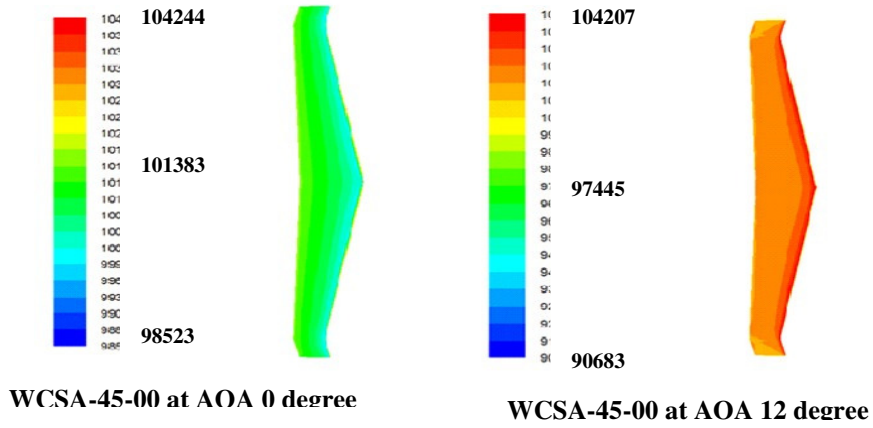
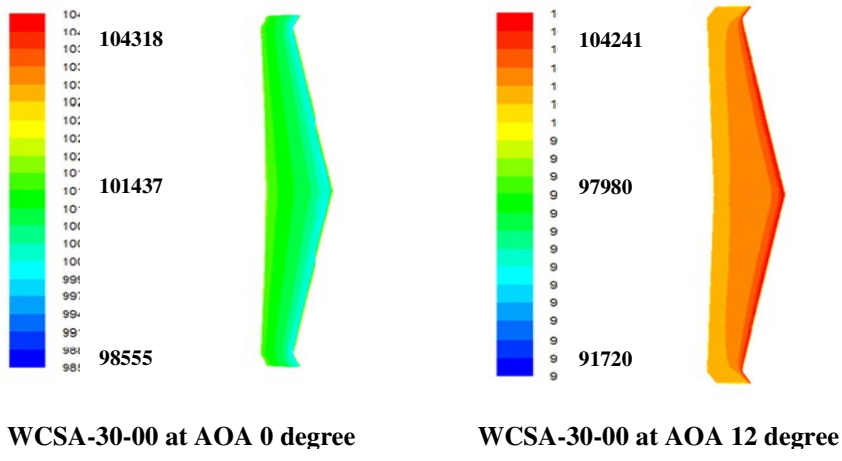
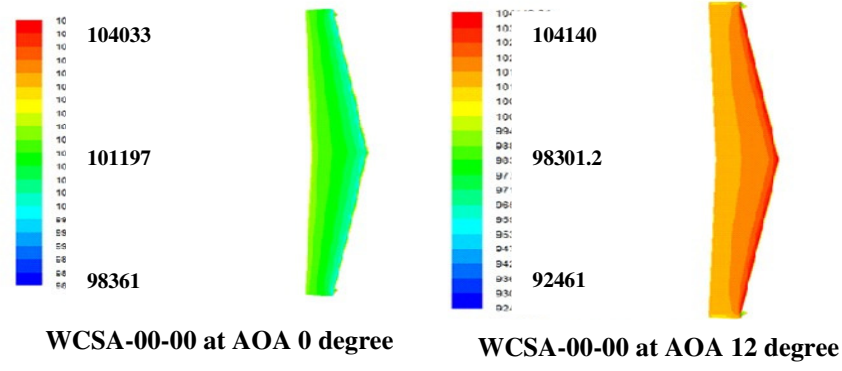


Fig. 13: Lower surface static pressure contours for Wing with winglet at cant angle 0, 30, 45 degree and sweep angle 0 degree with M=0.2 at sea level.

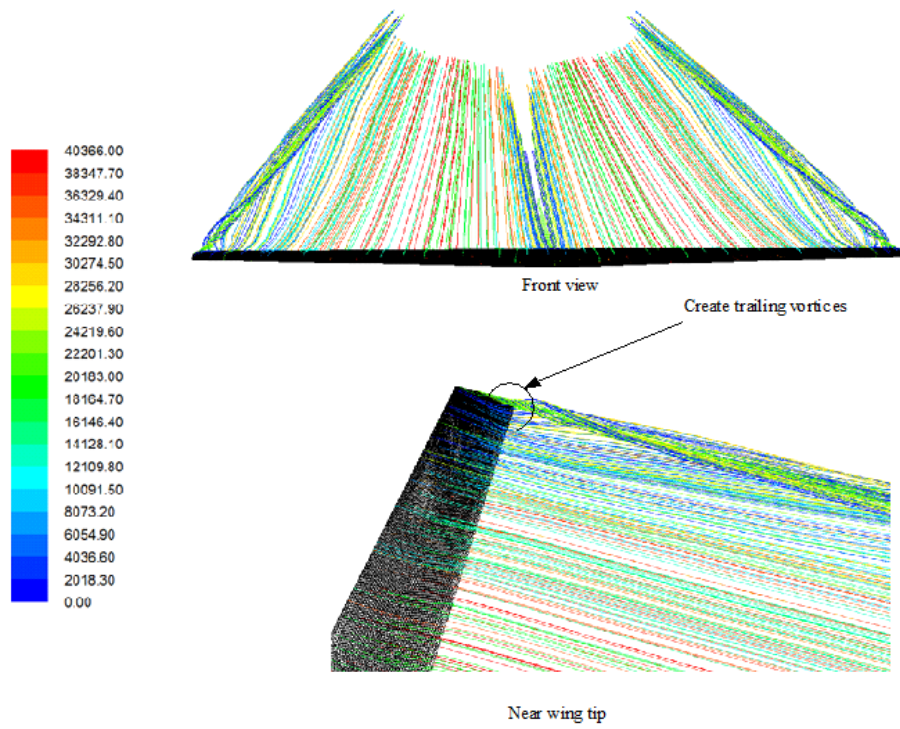


Fig. 14: Particle pathlines in case wing without winglet at angle of attack 12 degree.

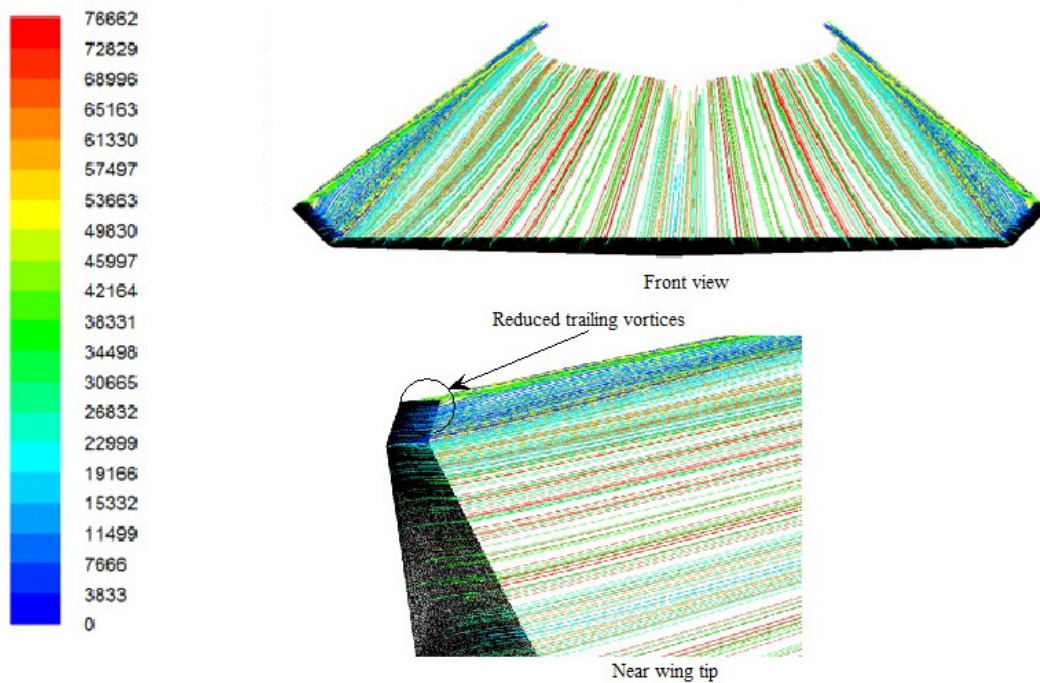


Fig. 15: Particle pathlines in case WCSA-45-40 at angle of attack 12 degree.